Spherical proton emitters

Sven Åberg
Department of Mathematical Physics, Lund Institute of Technology, P.O. Box 118 S-221 00 Lund, Sweden and Joint Institute for Heavy Ion Research, Oak Ridge National Laboratory, P.O. Box 2008, Oak Ridge, Tennessee 37831

Paul B. Semmes
Physics Department, Tennessee Technological University, Box 5051, Cookeville, Tennessee 38505

Witold Nazarewicz
Department of Physics, University of Tennessee, Knoxville, Tennessee 37996; Physics Division, Oak Ridge National Laboratory, P.O. Box 2008, Oak Ridge, Tennessee 37831; and Institute of Theoretical Physics, Warsaw University, ul. Hoża 69, PL-00681, Warsaw, Poland
(Received 4 June 1997)

Various theoretical approaches to proton emission from spherical nuclei are investigated, and it is found that all the methods employed give very similar results. The calculated decay widths are found to be qualitatively insensitive to the parameters of the proton-nucleus potential, i.e., changing the potential parameters over a fairly large range typically changes the decay width by no more than a factor of ~ 3. Proton half-lives of observed heavy proton emitters are, in general, well reproduced by spherical calculations with the spectroscopic factors calculated in the independent quasiparticle approximation. The quantitative agreement with experimental data obtained in our study requires that the parameters of the proton-nucleus potential be chosen carefully. It also suggests that deformed proton emitters will provide invaluable spectroscopic information on the angular momentum decomposition of single-proton orbitals in deformed nuclei. [S0556-2813(97)00410-X]

PACS number(s): 23.50.+z, 21.10.Jx, 21.10.Tg, 24.10.Eq

I. INTRODUCTION

Nuclei beyond the proton drip line are ground-state proton emitters. That is, the parent nucleus, ${}^{A+1}_{Z+1}X$, is unstable to the proton decay:

$$ {}^{A+1}_{Z+1}X \rightarrow {}^{A}_{Z}X + p. \tag{1}$$

Initially, the parent nucleus is in a quasistationary state, and the proton decay may be considered as a process where the proton tunnels through the potential barrier. In most cases, the combined Coulomb and centrifugal potentials give rise to barriers which are as large as ~ 15 MeV. Consequently, the associated lifetimes, ranging from 10^{-6} s to a few seconds, are sufficiently long to obtain a wealth of spectroscopic information. Experimentally, a number of proton emitters have now been discovered in the mass regions $A \sim 110$, 150, and 160 (see Refs. [1–4] and references quoted therein), and recently the first proton emitter above lead was reported [5]. It is anticipated that new regions of proton-unstable nuclei will be explored in the near future using radioactive nuclear beams.

The main objective of this paper is to perform systematic calculations of half-lives and spectroscopic properties of spherical ground-state proton emitters. We also discuss the reliability of different theoretical approaches, such as the distorted wave Born approximation, the two-potential approach, and the simple description of the barrier penetration problem in terms of one-dimensional quasiclassical method.

The paper is organized in the following way. In Sec. II the theoretical approaches used in this study are briefly presented. A comparison between models is given in Sec. III and the dependence of the calculated half-lives on model parameters is discussed in Sec. IV. Results of calculations are confronted with experiment in Sec. V. Finally, Sec. VI contains the main conclusions of the paper.

II. THEORETICAL APPROACHES

Proton emitters are extremely narrow resonances which can be interpreted in terms of isolated quasistationary states. Because of their extremely small widths, the perturbative approach based on standard reaction theory [6–8] is expected to be very accurate. The ground-state proton emission can be considered as one specific reaction channel [Eq. (1)], characterized by the transition amplitude $T_{A+1,Z+1;A,Z}$.

The resonance width can be expressed through the transition amplitude as [6,9]

$$\Gamma = 2\pi |T_{A+1,Z+1;A,Z}|^2, \tag{2}$$

where the transition amplitude, in the distorted-wave Born approximation (DWBA) is given by

$$T_{A+1,Z+1;A,Z} = \langle \psi_{Ap} \Psi_{Ap} | V_{Ap} | \Psi_{A+1} \rangle. \tag{3}$$

In Eq. (3) ψ_{Ap} is the incoming spherical wave representing the relative motion of the proton with respect to the daughter nucleus, Ψ_{Ap} is the product of *intrinsic* wave functions of the proton and the daughter, Ψ_{A+1} is the metastable state of the parent nucleus, and V_{Ap} is the interaction between the proton and the daughter nucleus.

For a given interaction V_{Ap}, one could in principle calculate the decay width directly by considering the time-reversed capture process, ${}^{A}X + p \rightarrow {}^{A+1}_{Z+1}X$ and study the asso-

ciated resonances. However, since the proton resonances are extremely narrow, $\Gamma \sim 10^{-22}-10^{-15}$ MeV, it is difficult to localize them numerically. Therefore, in our paper, we shall evaluate the transition amplitude explicitly using Eq. (3). (It is worth noting that in Ref. [10] an attempt was made to calculate the decay width directly by solving the Schrödinger equation in the complex plane; the imaginary part of a positive-energy Gamow resonance gives the decay width [11,12].)

Once the decay width is calculated, the half-life of the proton decay is obtained as

$$t_{1/2}=\frac{\hbar}{\Gamma}\ln 2. \tag{4}$$

As mentioned above, the proton resonances in question are extremely narrow and correspond to half-lives, $t_{1/2}\sim 10-10^{-6}$ s.

For calculating Γ we shall use three different methods: (i) DWBA as described in Sec. II A, (ii) the modified two-potential approach of Gurvitz [13], described in Sec. II B, and (iii) semiclassical approximation described in Sec. II C. The model parameters employed are specified in Sec. II D.

A. The DWBA method

The DWBA calculation of the decay width [Eq. (2)] requires knowledge of the (quasistationary) initial state wave function, Ψ_{A+1}, the final state wave functions, $\Psi_{Ap}\psi_{Ap}$, and the interaction potential. The interaction V_{Ap} in principle consists of a sum of two-body terms describing the pairwise interactions between the outgoing proton and all the A nucleons in the daughter nucleus. As is often done in DWBA [6–8] we shall approximate the ''true'' interaction V_{Ap} with the much simpler one-body potential V,

$$V=V_N+V_C, \tag{5}$$

which is a sum of a simple nuclear optical potential V_N and the Coulomb potential V_C. Using the Gell-Mann, Goldberger transformation [6–8], Eq. (3) can be rewritten as [9]

$$T_{A+1,Z+1;A,Z}=\langle \Psi_{Ap}\psi^C_{Ap}|V-V^0_C|\Psi_{A+1},\rangle, \tag{6}$$

where ψ^C_{Ap} is a scattering wave function corresponding to the point-charge Coulomb potential (i.e., a positive-energy eigenstate of the Hamiltonian $T+V^0_C$ where $V^0_C=Ze^2/r$).

The remaining part of the interaction, $V-V^0_C$, consists of the nuclear optical potential V_N and the correction δV^C to the Coulomb potential due to the finite charge distribution:

$$T_{A+1,Z+1;A,Z}=\langle \Psi_{Ap}\psi^C_{Ap}|V_N+\delta V^C|\Psi_{A+1}\rangle. \tag{7}$$

The wave function Ψ_{Ap} can be written as a product of the intrinsic wave function of the proton (the proton is assumed to be in its ground state) and that of the daughter nucleus, Φ_A, which in our work is treated as an inert core. The radial part of ψ^C_{Ap} is

$$\psi_{\ell}(r)=\sqrt{\frac{2\mu}{\pi\hbar^2 k}}\frac{F_{\ell}(r)}{r}, \tag{8}$$

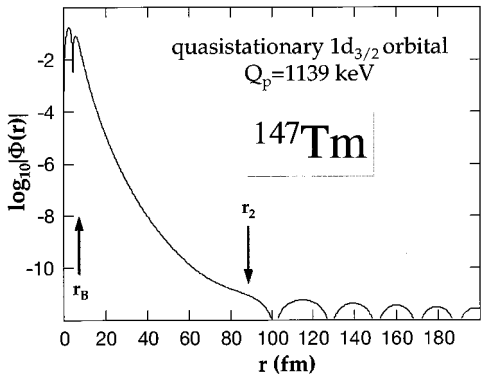

FIG. 1. Spherical radial wave function of the quasistationary $1d_{3/2}$ state at $Q_p=1139$ keV in ^{147}Tm (in logarithmic scale) as a function of r. The Coulomb barrier radius, $r_B=7$ fm, and the outer classical turning point, $r_2=87$ fm, are indicated.

where $k=\sqrt{2\mu E}/\hbar$, μ is the reduced mass, and F_{ℓ} is the regular Coulomb function. The k-dependent factor in Eq. (8) guarantees proper normalization of the scattering function ψ (cf. Refs. [14,15]).

The initial state wave function, Ψ_{A+1}, describes the proton quasibound to the core. This wave function can be written as a product of the daughter-nucleus wave function, Φ_A, and the proton wave function. The radial wave function of the proton in the quasibound state,

$$\Phi_{n\ell j}(r)=\frac{\phi_{n\ell j}(r)}{r}, \tag{9}$$

is found by numerically integrating the Schrödinger equation with the one-body potential (5) using the code ABMQ of de Vries [16]. The quasibound proton wave function $\phi_{n\ell j}(r)$ is found by joining smoothly the wave function from the interior region with the irregular part of the Coulomb wave function, $G_{\ell}(r)$, that asymptotically describes the proton wave function as $r\to\infty$. In our study, we assume that the nuclear interaction between the proton and the core, V_N, consists of a central and a spin-orbit potential of a Woods-Saxon type. For fixed Woods-Saxon radius and diffuseness, and for given energy, E, and quantum numbers $n\ell j$ of the quasibound state, the depth of the nuclear potential is iteratively adjusted until the inner and outer wave functions are smoothly connected. During the variation, the depth of the spin-orbit potential is also adjusted accordingly (see Sec. II D).

As an example, the calculated wave function $\Phi_{n\ell j}(r)$ of the quasistationary $1d_{3/2}$ state in ^{147}Tm is shown in Fig. 1. As expected, in the interior region ($r<7$ fm) the wave function has one node. The outer turning point is quite distant, at about 87 fm. This results in a reduction of the wave function in the barrier region by about 10 orders of magnitude. In the outer region, outside the classical outer turning point, the characteristic oscillatory behavior of the Coulomb function is seen.

By combining Eqs. (7), (8), and (9), the resonance width becomes

$$\Gamma=\frac{4\mu}{\hbar^2 k}\left|\int_0^\infty F_{\ell}(r)(V_N+\delta V^{\mathrm{Coul}})\phi_{n\ell j}(r)dr\right|^2. \tag{10}$$

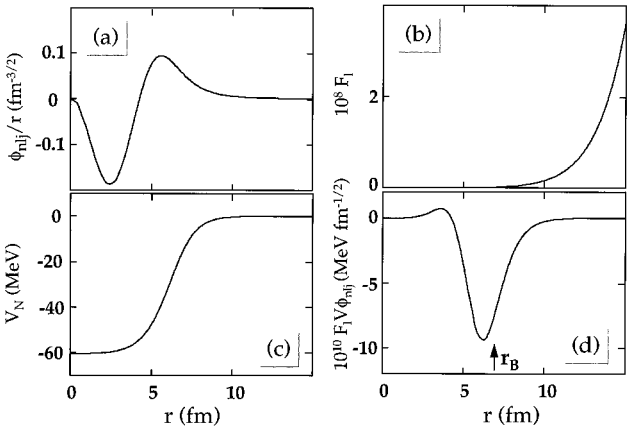

FIG. 2. Different terms contributing to the proton decay rate of the $1d_{3/2}$ state in ^{147}Tm shown in Fig. 1: (a) the radial wave function, (b) the regular Coulomb wave function, and (c) the proton potential V_N. In (d) the integrand of Eq. (10) is shown. The barrier radius is at $r_B=7$ fm. The resulting resonance width is 2.65×10^{-18} MeV.

Figures 2(a)–2(c) illustrate the radial dependence of the three terms in the integrand of Eq. (10): the quasibound wave function, $\Phi_{n\ell j}(r)$, the (regular) Coulomb function, $F_\ell(r)$, and the optical potential, V_N. The total integrand is shown in Fig. 2(d). The main contribution to the resonance width is seen to come from the surface region, and the integrand has a large peak around the Coulomb barrier radius, r_B. This is because the Coulomb function is vanishingly small at small r values, while the wave function of the quasistationary state decreases exponentially in the barrier region (cf. Fig. 1). The proton decay rate is thus expected to depend rather weakly on the detailed structure of the wave function in the interior part of the nucleus, while surface properties may be important.

B. The two-potential approach

Another perturbative method for calculating the decay width of an isolated quasistationary state is a modified two-potential approach introduced by Gurvitz and Kalbermann [17,13]. A short description of this method is given in the following; the details and examples can be found in Ref. [13] (see also Ref. [18]).

The particle with an energy $E>0$ moves in an effective potential $V(r)$ with a barrier [see Fig. 3(a)]. Since one considers a quasistationary state, the energy E is considerably lower than the barrier height V_B [$V_B=V(r_B)$ and r_B is the barrier radius]. The effective spherical potential $V(r)$ *includes the centrifugal term*, and thus the barrier height depends explicitly on the single-particle orbital angular momentum. The potential $V(r)$ can be formally split into two parts

$$V(r)=U(r)+W(r), \tag{11}$$

where

$$U(r)=\begin{cases} V(r) & \text{if } r\leqslant r_B, \\ V_B & \text{if } r>r_B, \end{cases} \tag{12}$$

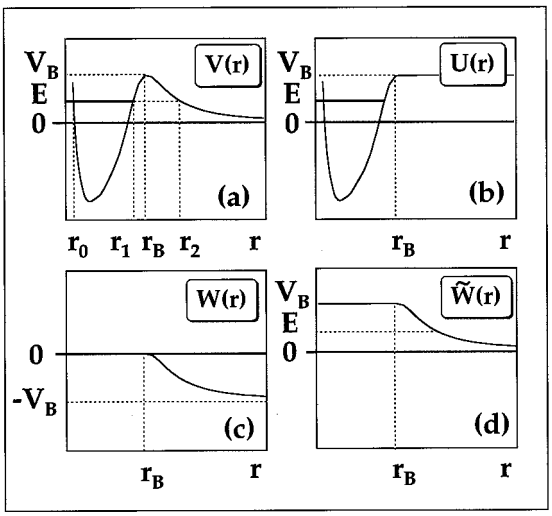

FIG. 3. The potentials appearing in the two-potential approach of Sec. II B: $V(r)$, $U(r)$ [Eq. (12)], $W(r)$ [Eq. (13)], and $\widetilde{W}(r)=W(r)+V_B$. r_B is the barrier radius, and r_0, r_1, and r_2 are the classical turning points.

and

$$W(r)=\begin{cases} 0 & \text{if } r\leqslant r_B, \\ V(r)-V_B & \text{if } r> r_B \end{cases} \tag{13}$$

as shown in Figs. 3(b) and 3(c). It is assumed that initially the particle occupies the bound eigenstate of the Hamiltonian H_0 with the potential $U(r)$,

$$H_0\Phi_0=\left(\frac{p_r^2}{2\mu}+U\right)\Phi_0=E_0\Phi_0. \tag{14}$$

The perturbing potential W disturbs the wave function Φ_0 and transforms it to a quasistationary state, an eigenstate of the full Hamiltonian $H=p_r^2/2\mu+V$ with an energy E. It is to be noted that the energies E and E_0 are not identical; except for some simple cases the energy shift

$$\Delta\equiv E-E_0 \tag{15}$$

is different from zero [13]. Since the perturbation $W(r)$ does not vanish at $r\to\infty$, in order to solve the eigenproblem perturbatively, one introduces a ''shifted'' perturbing potential $\widetilde{W}(r)=W(r)+V_B$ shown in Fig. 3(d). By construction, this potential vanishes for $r\to\infty$.

In the TPA one obtains a simple expression for the decay width

$$\Gamma=\frac{4\mu}{\hbar^2 k}\left|\int_{r_B}^{\infty}\phi_{n\ell j}(r)W(r)\chi_\ell(r)dr\right|^2, \tag{16}$$

where $k=\sqrt{2\mu E_0}/\hbar$, $\phi_{n\ell j}(r)$ is the radial wave function of Φ_0, and $\chi_\ell(r)$ is the regular radial wave function of the Hamiltonian $T+\widetilde{W}$, with the asymptotic behavior

$$\chi_\ell(0)=0$$

and

$$\chi_{\ell}(r)\rightarrow \sin(kr-\pi\ell/2+\delta_{\ell}) \quad \text{for } r\rightarrow\infty. \tag{17}$$

Since for $r>r_B$ the radial wave function $\phi_{n\ell j}(r)$ is

$$\phi_{n\ell j}(r)=\phi_{n\ell j}(r_B)\exp[-\alpha(r-r_B)], \tag{18}$$

the integral (16) can be carried out analytically, and the final result is [17,13]

$$\Gamma=\frac{\hbar^2}{\mu k}|\phi_{n\ell j}(r_B)[\alpha\chi_{\ell}(r_B)+\chi'_{\ell}(r_B)]|^2, \tag{19}$$

where $\alpha=\sqrt{2\mu(V_B-E_0)}/\hbar$. Note that in the TPA, the contribution to the integral Eq. (16) comes entirely from the region $r>r_B$, but the final result Eq. (19) depends only on the values of the wave functions at r_B. However, as discussed in Ref. [13], the final result for Γ does not depend on the particular choice of r_B.

The regular scattering wave function χ_{ℓ} is

$$\chi_{\ell}(r)=\chi_{\ell}(r_B)\frac{\sinh(\alpha r)}{\sinh(\alpha r_B)} \quad \text{if } r<r_B, \tag{20a}$$

$$\chi_{\ell}(r)=\cos\delta_{\ell}F_{\ell}(kr)-\sin\delta_{\ell}G_{\ell}(kr) \quad \text{if } r>r_{\text{big}}, \tag{20b}$$

where F_{ℓ} and G_{ℓ} are the regular and irregular Coulomb wave functions, respectively, and r_{big} is the cutoff radius beyond which the contribution from the nuclear potential is unimportant. In practice this is fulfilled for $r_{\text{big}}>1.5r_B$. In the intermediate region $r_B<r<r_{\text{big}}$ the scattering wave function was obtained by the direct integration of the Schrödinger equation. The relative phase δ_{ℓ} was calculated by matching logarithmic derivatives at $r=r_{\text{big}}$.

A simple approximation to Eq. (19) can be obtained by neglecting the nuclear contribution to the scattering state for $r>r_B$, i.e., by assuming that for $r>r_B$ χ_{ℓ} is given by Eq. (20b). In this case, the phase shift is given by

$$\tan\delta_{\ell}=\frac{kF'_{\ell}(kr_B)-\alpha\coth(\alpha r_B)F_{\ell}(kr_B)}{kG'_{\ell}(kr_B)-\alpha\coth(\alpha r_B)G_{\ell}(kr_B)}. \tag{21}$$

In the following, this approximation will be referred to as TPA1. Yet another approximation (TPA2), used, e.g., in Ref. [19], consists in replacing $\chi_{\ell}(r)$ with $F_{\ell}(r)$. In this case, only the bound-state wave function $\phi_{n\ell j}$ is calculated numerically.

C. The quasiclassical method

For low-lying metastable states, the quasiclassical method (WKB) is expected to work very well. The quasiclassical expressions for Γ and Δ can be derived from the TPA [13]. In particular, the decay width can be written as

$$\Gamma=\mathcal{N}\frac{\hbar^2}{4\mu}\exp\left\{-2\int_{r_1}^{r_2}|k(r)|dr\right\}, \tag{22}$$

where

$$\hbar k(r)=\sqrt{2\mu[E-V(r)]} \tag{23}$$

is the classical momentum, r_i $(i=0,1,2)$ are the classical turning points [Fig. 3(a)], and $E=Q_p$. The normalization factor $\mathcal{N}$ is usually evaluated by considering the classically allowed region only:

$$\mathcal{N}^{-1}=\int_{r_0}^{r_1}\frac{dr}{k(r)}\cos^2\left(\int_{r_0}^{r}k(r')dr'-\frac{\pi}{4}\right). \tag{24}$$

However, as noted in Ref. [13], the contribution to the norm from the classically forbidden region should in principle also be considered. Often, the cosine term in Eq. (24) is approximated by its average value of 1/2, giving

$$\overline{\mathcal{N}^{-1}}=\frac{1}{2}\int_{r_0}^{r_1}\frac{dr}{k(r)}. \tag{25}$$

In the following, this approximation shall be referred as to WKB1. Because of its simplicity the WKB approach has been widely used to study spherical proton emitters (see, e.g., Ref. [20]).

TABLE I. Woods-Saxon parameters (radius R_0 and diffuseness a) used in the calculations. The total radius R_0, is given by $r_0A^{1/3}$. All parameters are in fm.

Parameter	WS1 [21]	WS2 [22]
r_0	1.17	1.275
a	0.75	0.70
$r_{0,\text{so}}$	1.01	1.32
a_{so}	0.75	0.70

D. Model parameters

In our calculations, the proton optical potential was approximated by an average Woods-Saxon (WS) field, containing the central term and the spin-orbit potential.

The WS form factor is defined by the radius, $R_0=r_0A^{1/3}$, and diffuseness a. Two separate sets of WS parameters have been considered: the Becchetti-Greenlees set proposed in Ref. [21] (set WS1) and the ''universal'' set of Refs. [22,23] (set WS2). The set WS1, which was mainly fitted to low-energy proton scattering data, has significantly smaller radii, and it has slightly larger surface diffuseness (see Table I). The set WS2 gives a very good reproduction of single-particle proton properties in deformed nuclei [24], but its radius seems to be overestimated [25].

The depth of the central potential, V_0, has not been taken from Refs. [21,22], but rather adjusted to reproduce the experimental energy of a quasistationary state. For the depth of the spin-orbit potential, we adopted a simple ansatz $V_{0,\text{so}}=-0.2V_0$. To facilitate a comparison between different theoretical approaches, the same values of V_0 were used in the DWBA and WKB calculations. Essentially the same values of V_0 were obtained in the TPA calculations (see Sec. III for more discussion regarding this point).

The Coulomb potential was approximated by that of the nuclear charge equal to Ze uniformly distributed inside the radius R_0.

TABLE II. Half-lives of proton emitters $t_{1/2}$ calculated with different theoretical models and with the WS1 set of optical model parameters [21]. The odd proton is assumed to fully occupy the specified spherical orbital $(n\ell j)$ (spectroscopic factor equal to one). For the odd-odd decays it is assumed that the neutron configuration remains the same in the parent and daughter nuclei. The calculation was carried out for average experimental Q_p values listed in second column. The abbreviations refer to the distorted wave Born approximation of Sec. II A [DWBA, Eq. (10)], the two-potential approach of Sec. II B [TPA, Eq. (19)], and the quasiclassical method of Sec. II C [WKB, Eqs. (22) and (24)]. In the TPA2 variant, the scattering wave function $\chi_\ell(r)$ has been replaced by the regular Coulomb wave function $F_\ell(r)$. In the WKB1 variant, the approximation (25) for the normalization constant has been used.

Nucleus	Q_p (keV)	Orbit	$t_{1/2}$				
			DWBA	TPA	TPA2	WKB	WKB1
$^{105}_{51}Sb_{54}$	491	$1d_{5/2}$	20 s	20 s	21 s	19 s	24 s
$^{109}_{53}I_{56}$	829	$1d_{5/2}$	10 μs	10 μs	11 μs	9 μs	12 μs
$^{112}_{55}Cs_{57}$	823	$1d_{5/2}$	68 μs	67 μs	72 μs	64 μs	80 μ s
$^{113}_{55}Cs_{58}$	977	$1d_{5/2}$	540 ns	540 ns	570 ns	510 ns	640 ns
$^{146}_{69}Tm_{77}$	1140	$0h_{11/2}$	350 ms	340 ms	380 ms	370 ms	530 ms
	1210	$0h_{11/2}$	53 ms	52 ms	58 ms	57 ms	81 ms
$^{147}_{69}Tm_{78}$	1071	$0h_{11/2}$	2.6 s	2.5 s	2.8 s	2.7 s	3.9 s
	1132	$1d_{3/2}$	210 μs	210 μs	220 μs	210 μs	260 μs
$^{150}_{71}Lu_{79}$	1283	$0h_{11/2}$	31 ms	30 ms	33 ms	33 ms	47 ms
$^{151}_{71}Lu_{80}$	1255	$0h_{11/2}$	60 ms	58 ms	64 ms	63 ms	90 ms
$^{156}_{73}Ta_{83}$	1028	$1d_{3/2}$	97 ms	96 ms	100 ms	96 ms	120 ms
	1130	$0h_{11/2}$	6.3 s	6.2 s	6.9 s	6.9 s	9.8 s
$^{157}_{73}Ta_{83}$	947	$2s_{1/2}$	220 ms	220 ms	230 ms	210 ms	170 ms
$^{160}_{75}Re_{85}$	1284	$1d_{3/2}$	230 μs	230 μs	250 μs	230 μs	290 μs
$^{161}_{75}Re_{86}$	1214	$2s_{1/2}$	190 μs	190 μs	200 μs	180 μs	145 μs
	1338	$0h_{11/2}$	86 ms	85 ms	94 ms	100 ms	150 ms
$^{165}_{77}Ir_{88}$	1733	$0h_{11/2}$	100 μs	100 μs	110 μs	110 μs	160 μs
$^{166}_{77}Ir_{89}$	1168	$1d_{3/2}$	21 ms	21 ms	22 ms	21 ms	27 ms
	1340	$0h_{11/2}$	280 ms	270 ms	290 ms	290 ms	410 ms
$^{167}_{77}Ir_{90}$	1086	$2s_{1/2}$	36 ms	36 ms	38 ms	35 ms	28 ms
	1261	$0h_{11/2}$	2.0 s	2.0 s	2.2 s	2.2 s	3.1 s
$^{171}_{79}Au_{92}$	1718	$0h_{11/2}$	350 μs	340 μs	380 μs	370 μs	530 μs
$^{185}_{83}Bi_{98}$	1611	$2s_{1/2}$	3.2 μs	3.1 μs	3.3 μs	3.1 μs	2.5 μs
	1611	$0h_{9/2}$	21 ms	20 ms	23 ms	23 ms	32 ms

III. COMPARISON BETWEEN MODELS

The half-lives of some known proton emitters calculated with the different theoretical methods described in Sec. II are given in Table II. The values of Q_p were taken from experiment; they include the recoil and screening corrections [1]. The quantum numbers $(n\ell j)$ characterizing the quasistationary state are also taken at the values suggested from original experimental papers. All half-lives are calculated assuming that a valence proton fully occupies the single-particle orbital $(n\ell j)$ in the parent nucleus, i.e., it was assumed that the spectroscopic factor $S_p = 1$. The detailed comparison between the calculated and measured half-lives is presented in Sec. V below, along with a discussion of the spectroscopic factors extracted from the data. The main aim of this section is to compare different variants of calculations.

As seen in Table II, different methods applied in our work give similar results. If one is satisfied with the order-of-magnitude estimate, the simplest WKB or WKB1 method is an excellent tool.

The half-lives obtained with the WKB method are within 10% of those with the DWBA. The WKB1 approximation is slightly less accurate, and gives half-lives up to $\sim 50\%$ longer than the DWBA result.

The TPA yields half-lives which are practically identical to those obtained with the DWBA. Even more remarkably, the TPA2 variant yields half-lives that are within 10% of the

TABLE III. Energy shifts $E - E_0$ and Δ [Eq. (26)] calculated for several quasistationary states shown in Table II.

Nucleus	Orbit	$E - E_0$ (keV)	Δ (keV)
^{109}I	$1d_{5/2}$	−2.7	−4.4
^{147}Tm	$0h_{11/2}$	−0.8	−1.7
^{156}Ta	$1d_{3/2}$	−0.8	−2.2
^{171}Au	$0h_{11/2}$	−0.9	−1.5
^{185}Bi	$2s_{1/2}$	+1.5	−2.1
^{185}Bi	$0h_{9/2}$	−0.1	−1.1

DWBA and TPA values. This result demonstrates that the further simplification of already simple analytic expressions by Gurvitz [13], based on replacing the scattering wave function χ_ℓ with the regular Coulomb wave function F_ℓ, is justified. The TPA1 variant [Eq. (21)] gives results that are extremely similar to those with TPA2. The fractional change in calculated half-lives between TPA1 and TPA2 is of the order of 0.1%, so the correction for the finite size of $\widetilde{W}(r)$ for $r<r_B$ can safely be neglected. The reason for this is the very small value of δ_ℓ. Indeed, according to Eq. (21), its magnitude is, roughly, governed by the ratio of F_ℓ/G_ℓ at $r=r_B$. That is, $\chi_\ell(r_B)\approx F_\ell(r_B)$ [cf. Eq. (20b) and discussion in Ref. [19]].

As discussed in Sec. II D, in the TPA calculations the depth of the central potential, V_0, has been adjusted to reproduce the experimental Q_p value. Formally, when making this adjustment, one should correct for the energy shift Δ between the energy E of the ''true'' quasistationary state (appearing in the DWBA model) and the ''bound-state'' energy E_0. This correction might be important in some cases, since the value of V_0 appears in the WKB exponent.

The energy shift can be estimated in the TPA as [13]

$$\Delta=-\frac{\hbar^2\alpha}{\mu k}|\phi_{n\ell j}(r_B)|^2[2\alpha\chi_\ell(r_B)\widetilde{\chi}_\ell(r_B)-k], \quad (26)$$

where $\widetilde{\chi}_\ell(r)$ is the *irregular* scattering wave function. An even simpler expression can be obtained in a quasiclassical limit:

$$\Delta=\frac{V'(r_B)}{4\alpha^2}|\phi_{n\ell j}(r_B)|^2. \quad (27)$$

That is, if $V'(r_B)=0$ [as in Fig. 3(a)] Δ is governed by higher-order corrections beyond the quasiclassical limit, hence expected to be very small. Table III displays a few selected examples of the values of the energy shift E-E_0, computed from the DWBA and TPA energy eigenvalues obtained with the same potential, and the estimate Δ, calculated by means of Eq. (26). The estimated shifts range from −1 keV to −5 keV, depending on ℓ (larger ℓ values give rise to smaller energy shifts) and E_0 (Δ increases with E_0). However, the true shifts E-E_0 are consistently smaller in magnitude than the estimates given by Δ. The half-lives calculated in the TPA using the same potential as the DWBA (and consequently with slightly different energy eigenvalues) were consistently smaller than the DWBA half-lives. The largest change occurred for the ^{109}I case, where the TPA half-life decreased by 9%; in the other cases, the calculated half-lives changed by 5% or less. These changes in the half-lives due to the energy shift seem larger than expected based on Ref. [13]. Nonetheless, the agreement with the DWBA half-lives is excellent when using the experimental Q_p values, which suggests that neglecting the difference between E and E_0 is a reasonable approach in practice for low-lying states such as those discussed in this work.

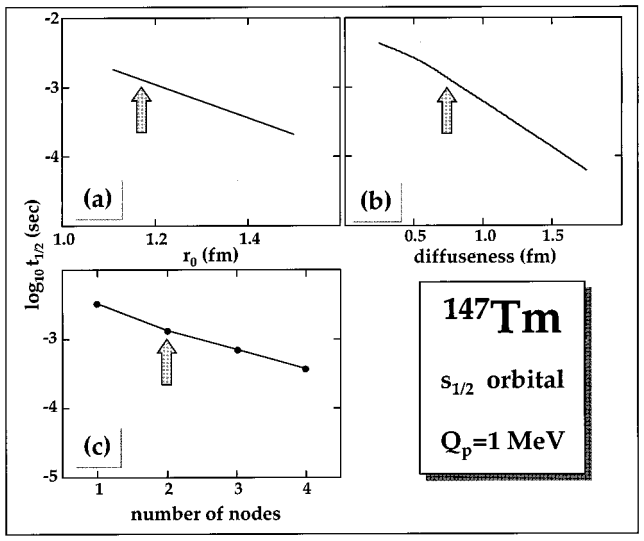

FIG. 4. Sensitivity of the calculated proton half-life of the $2s_{1/2}$ state in ^{147}Tm on model parameters: potential radius (a) and diffuseness (b). Portion (c) illustrates the dependence of $t_{1/2}$ on the number of nodes of the proton wave function. The calculations are performed within the DWBA formalism and at a fixed value of $Q_p=1$ MeV. The standard values of parameters are marked by arrows.

IV. SENSITIVITY OF RESULTS TO THE OPTICAL MODEL PARAMETERS

In order to investigate the sensitivity of the calculated half-lives to the choice of parameters of proton-nucleus potential, the DWBA calculations have been performed for different WS potentials.

Figure 4 illustrates the sensitivity of the calculated half-lives to the physically relevant optical model parameters, namely, the radius R_0 [Fig. 4(a)] and diffuseness a [Fig. 4(b)]. In addition, to check the sensitivity of the results on the details of radial wave function in the nuclear interior, in Fig. 4(c) the number of radial nodes in the the proton wave function has been artificially varied by adjusting the depth of the central potential V_0. In each case, the angular momentum and the Q_p value were held constant ($\ell=0$ and $Q_p=1$ MeV). The results presented in Fig. 4 confirm the previous conclusion of Ref. [3] (cf. Refs. 35 and 36 quoted therein). Namely, variation of the optical model parameters within the ranges of their uncertainties affects the predicted half-lives by not much more than a factor of about three. For example, if the radius r_0 is changed from the standard value 1.17 fm to the (unrealistically) large value of 1.4 fm, the half-life decreases by a factor of about 3 to 4. Similarly, if the diffuseness is increased by 50% from its standard value of $a=0.75$

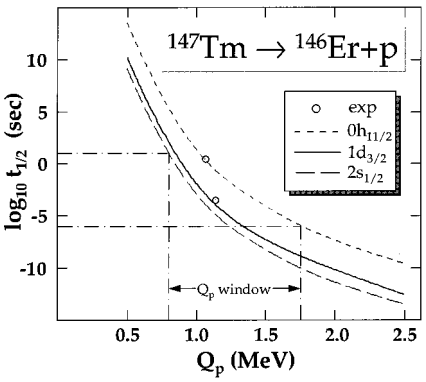

FIG. 5. Proton partial decay half-lives for $2s_{1/2}$, $1d_{3/2}$, and $0h_{11/2}$ states in in ^{147}Tm as a function of Q_p calculated in the DWBA model. Experimental half-lives are indicated.

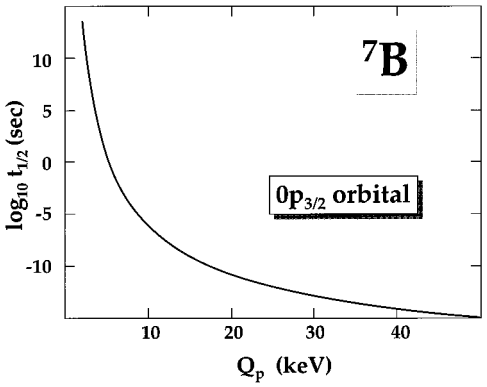

FIG. 6. Proton partial decay half-life for the $0p_{3/2}$ state in ^{7}B versus Q_p.

fm, the half-life decreases by a factor of 3. Also, very minor changes in the half-life are found as a function of the number of nodes of the radial proton wave function.

The weak sensitivity of $t_{1/2}$ to the details of the optical proton potential has been discussed in Ref. [26] in the context of two-proton radioactivity. It has been shown that more than 94–99 % of the WKB exponent, $\int_{r_1}^{r_2} dr\ |k(r)|$, comes from the region $r > r_B$, which is almost solely determined by the combined Coulomb+centrifugal interaction. Consequently, a rough estimate of $t_{1/2}$ can be obtained by ignoring the nuclear structure details.

The sensitivity to particular parameter sets of the WS potential has been studied by performing a second set of DWBA calculations with the parameter set WS2 (see Table I). The half-lives obtained with the set WS2 are systematically smaller as compared to those with the set WS1 by a factor of $\sim$ 2–3. This result can be directly attributed to the slightly too large potential radius in the ''universal'' set WS2 (cf. discussion in Sec. II D). Indeed, according to a simple WKB estimate [27,28], the ratio of half-lives in both WS models depends on R_0 as:

$$\ln\left(t_{1/2}^{\mathrm{WS1}}/t_{1/2}^{\mathrm{WS2}}\right) \propto \sqrt{R_0^{\mathrm{WS2}}} - \sqrt{R_0^{\mathrm{WS1}}} > 0. \tag{28}$$

For a quantitative comparison between calculated and experimental half-lives, this difference of a factor of $\sim$2–3 between the sets WS1 and WS2 is unacceptable. Consequently, we regard the set WS1 as more appropriate for the pure single-particle decay rate calculations. However, the set WS2 seems to be more appropriate for calculating detailed structure effects (e.g., for estimating the theoretical spectroscopic factors).

The very strong dependence of the proton half-life on the Q_p value and angular momentum is well known (e.g., see Refs. [1,3]). For completeness, proton partial decay half-lives calculated in the DWBA are presented in Fig. 5 for the $2s_{1/2}$, $1d_{3/2}$, and $0h_{11/2}$ states in ^{147}Tm as a function of Q_p. As the Q_p value changes from 0.5 MeV to 2.5 MeV, the half-life changes by more than 22 orders of magnitude, from 10^{10} s to 10^{-12} s for the decay from the $1d_{3/2}$ state. For small values of Q_p, proton-emission half-lives are very long and the total half-life is completely dominated by β decay. For large Q_p values, proton-emission half-lives are prohibitively short to allow experimental observation of an individual decay. Hence, from the spectroscopic point of view, the size of the Q_p window of interest is rather narrow; for a typical rare-earth nucleus it is about 0.8–1.7 MeV, see Fig. 5.

The three curves in Fig. 5 corresponding to different orbital angular momentum are clearly separated, reflecting the importance of the centrifugal barrier. This strong dependence on angular momentum facilitates the identification of the proton wave function in the parent nucleus from measured half-lives and Q_p values. Proton emission has been observed from two different states in ^{147}Tm [1,29], and the corresponding experimental values are shown in Fig. 5. The proton configurations have been assigned in Refs. [1,29] as $0h_{11/2}$ and $2d_{3/2}$, and their half-lives agree nicely with the calculated values.

So far, ground-state proton radioactivity has not been observed in the very light nuclei. One reason is the extremely narrow Q_p window due to the low Coulomb barrier. For instance, as discussed in Ref. [30], for nuclei around $Z=20$ the half-life window of 10 to 10^{-4} s corresponds to proton energies of 100–150 keV. For lighter nuclei this effect is even more dramatic. Figure 6 shows the calculated proton half-life for the $0p_{3/2}$ state in ^{7}B as a function of Q_p. As the Q_p value is varied between 3 to 50 keV the half-life varies over 30 decades! The window of Q_p values corresponding to possibly observable proton decay is thus 5–10 keV.

Although ground-state proton radioactivity is unlikely to be observed in light nuclei, it is nonetheless interesting to study how the effect of a proton halo [31] would affect the decay half-life. In this work, a proton halo has been simulated by making the diffuseness unusually large. For example, if the diffuseness parameter is increased from its standard value of $a=0.75$ fm to $a=1.5$ fm, the proton wave function of the $0p_{3/2}$ state is effectively pushed out, and the root-mean-square radius changes from 5 fm to 7 fm [see Fig. 7(a)]. As a result, the half-life for proton emission decreases. However, as shown in Fig. 7(b), the effect of ''halo'' is much smaller than what one might expect; the proton half-life changes only by a factor of $\sim$3. This result is consistent with the earlier conclusions: the values of $t_{1/2}$ show rather weak sensitivity to details of nuclear structure.

V. COMPARISON WITH EXPERIMENT

Table IV displays the single-proton emission half-lives ($t_{1/2}^{\mathrm{th}}$) calculated with the DWBA method with the parameter

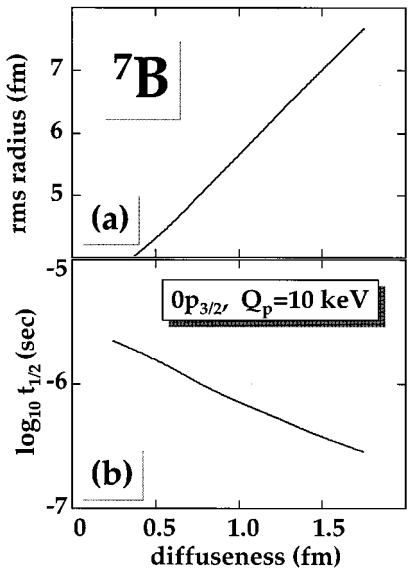

FIG. 7. Root-mean-square-radius of the $0p_{3/2}$ quasistationary state in ^{7}B at $Q_p=10$ keV as a function of diffuseness of the WS potential (a); the corresponding half-lives (b).

set WS1, together with experimental half-lives ($t_{1/2}^{\rm exp}$). The uncertainties in the calculated half-lives are estimated directly from the experimental uncertainties in the Q_p values. Note that no attempt has been made to estimate any uncertainty in the calculated half-lives due to uncertainties in the parameters of the optical model potential, and thus the error bar on the calculated half-lives should be considered as a lower limit.

The experimental spectroscopic factors can be determined as ratios of calculated and measured half-lives [3]

$$S_p^{\rm exp}=t_{1/2}^{\rm th}/t_{1/2}^{\rm exp}. \tag{29}$$

Theoretically, the spectroscopic factor, defined as [32,33]

$$S_p=\frac{1}{2I_i+1}|\langle I_i\|a^\dagger_{n\ell j}\|I_f\rangle|^2, \tag{30}$$

measures the fragmentation of a single-particle orbital ($n\ell j$). The proton emission is analogous to the pick-up reaction: a proton with angular momentum j is removed from the parent nucleus with angular momentum I_i leading to the final state in the daughter system with $I=I_f$.

Spectroscopic factors can easily be calculated in the independent-quasiparticle approximation (BCS), in which one assumes that the ground state of an odd-Z nucleus is a one-quasiparticle state, while that of an odd-odd system is a two-quasiparticle configuration. In the BCS theory, the spectroscopic factor is given by [34,33]

$$S_p^{\rm th}=u_j^2, \tag{31}$$

where u_j^2 is the probability that the spherical orbital ($n\ell j$) is empty in the daughter nucleus. This expression assumes that the even-even (or odd-N) core does not change during the decay process (for instance, the odd neutron on the odd-odd proton emitter is considered as a passive spectator). Under this assumption, expression (31) is valid for both the even-N and odd-N nuclei. Note that the maximum and minimum values for S_p in this approach are 1 and 0, corresponding to a completely empty or a completely filled single-particle orbital ($n\ell j$) in the daughter nucleus.

The spectroscopic factors extracted from the data are shown in Table IV. Except for the cases of ^{113}Cs and ^{185}Bi, essentially all the experimental spectroscopic factors are between 0.1 and 1; only for ^{146}Tm the extracted value of S_p is greater than 1, but the experimental uncertainty in this case is large.

The BCS calculations were carried out with the monopole pairing Hamiltonian of Ref. [35]. Specifically, the proton pairing strength constant was taken as

$$G_p=\frac{1}{A}[17.9+0.176(N-Z)], \tag{32}$$

and the pairing-active space consisted of the lowest Z (doubly degenerate) single-particle proton levels. Here, we applied the single-particle model of Ref. [24], with parameter set WS2. This model has proved to be very successful in reproducing properties of single-proton states of rare-earth nuclei.

The correlation between experimental and theoretical spectroscopic factors is shown in Fig. 8. For odd-Z, N-even ground-state proton emitters the agreement between experiment and theory is good. For the two cases indicated by stars, ^{109}I and ^{113}Cs, the experimental values fall well below theoretical predictions. This suggests the strong fragmentation of the single-particle strength and/or increased tunneling probability as compared to spherical predictions. Figure 9 shows calculated equilibrium quadrupole deformations of Refs. [36] (finite-range droplet model, FRDM) and [37] (extended Thomas-Fermi with Strutinsky integral model, ETFSI) along the trajectory of known proton emitters, $Z\approx 0.74N+12$ [2]. Indeed, both ^{109}I and ^{113}Cs are predicted to be deformed, and the ''anomalous'' proton half-life of ^{109}I has been reproduced by deformed calculations of Refs. [38–40].

Recently, a similar analysis of spectroscopic factors has been performed in Ref. [41] using the quasiclassical approximation to calculate $t_{1/2}$ and to extract experimental spectroscopic factors. The authors assumed the exact degeneracy of the $0h_{11/2}$, $1d_{3/2}$, and $2s_{1/2}$ shells. In this approximation, the number of pairing-active states is 18. The occupation coefficients can be computed from the particle-number equation:

$$18v^2=18-2p, \tag{33}$$

where p is the number of proton hole pairs counting down from $Z=82$. The resulting orbital-independent spectroscopic factor is given by

$$\tilde{S}_p^{\rm th}=u^2=1-v^2=\frac{p}{9}, \tag{34}$$

that is, it is 0.11 for Tl, 0.22 for Au, 0.33 for Ir, and so on. Comparing with the values of $S_p^{\rm th}$ in Table IV, one can see that the ''supershell'' approximation of Eq. (34) is rather crude, and the single-particle degeneracy should be considered when computing theoretical spectroscopic factors.

TABLE IV. Experimental ($t_{1/2}^{\rm exp}$) and calculated ($t_{1/2}^{\rm th}$) half-lives of ground-state proton emitters. The theoretical half-lives are calculated within the DWBA method using the WS1 parameter set and taking experimental Q_p values, and the odd proton is assumed to occupy fully the spherical orbital ($n\ell j$). Experimental spectroscopic factors, $S_p^{\rm exp}$ [Eq. (29)], are compared to those obtained in the BCS theory, $S_p^{\rm th}$ [Eq. (31)]. The error in calculated half-lives comes from uncertainty in experimental Q_p.

Nucleus	Q_p (keV)	Orbit	$t_{1/2}^{\rm exp}$	$t_{1/2}^{\rm th}$	$S_p^{\rm exp}$	$S_p^{\rm th}$
$^{109}_{53}I_{56}$	829 ±4	$1d_{5/2}$	(100 ±5) μs [29]	(10 ±1) μs	0.10 ±0.01	0.76
$^{112}_{55}Cs_{57}$	823 ±7	$1d_{5/2}$	(500 ±100) μs [43]	(68 ±17) μs	0.14 ±0.04	0.59
$^{113}_{55}Cs_{58}$	977 ±4	$1d_{5/2}$	(17 ±2) μs [43]	(0.540 ±0.06) μs	0.032 ±0.005	0.59
$^{146}_{69}Tm_{77}$	1140 ±5	$0h_{11/2}$	(235 ±27) ms [44]	(350 ±50) ms	1.5 ±0.3	0.64
	1210 ±5	$0h_{11/2}$	(72 ±23) ms [44]	(53 ±7) ms	0.74 ±0.26	0.64
$^{147}_{69}Tm_{78}$	1071 ±3	$0h_{11/2}$	$(2.7\ ^{+2.4}_{-0.9})$ s [45]	(2.6 ±0.2) s	0.9 ±0.7	0.64
	1132 ±4	$1d_{3/2}$	(360 ±40) μs [29]	(210 ±20) μs	0.58 ±0.09	0.79
$^{150}_{71}Lu_{79}$	1283 ±4	$0h_{11/2}$	$(40\ ^{+30}_{-20})$ ms [29]	(31 ±3) ms	0.8 ±0.5	0.54
$^{151}_{71}Lu_{80}$	1255 ±3	$0h_{11/2}$	$(130\ ^{+160}_{-50})$ ms [29]	(60 ±5) ms	0.5 ±0.4	0.54
$^{156}_{73}Ta_{83}$	1028 ±5	$1d_{3/2}$	(144 ±24) ms [46]	(97 ±17) ms	0.67 ±0.16	0.67
	1130 ±8	$0h_{11/2}$	(8.9 ±2.3) s [46]	(6.3 ±1.5) s	0.71 ±0.25	0.44
$^{157}_{73}Ta_{84}$	947 ±7	$2s_{1/2}$	(300 ±110) ms [47]	(220 ±60) ms	0.74 ±0.34	0.66
$^{160}_{75}Re_{85}$	1284 ±6	$1d_{3/2}$	(870 ±200) μs [42]	(230 ±40) μs	0.26 ±0.07	0.58
$^{161}_{75}Re_{84}$	1214 ±6	$2s_{1/2}$	(370 ± 40) μs [47]	(190 ±30) μs	0.51 ±0.10	0.59
	1338 ±7	$0h_{11/2}$	(325 ± 44) ms [47]	(86 ±14) ms	0.27 ±0.06	0.33
$^{165}_{77}Ir_{88}$	1733 ±7	$0h_{11/2}$	(350 ±70) μs [41]	(100 ±10) μs	0.29 ±0.07	0.23
$^{166}_{77}Ir_{89}$	1168 ±8	$1d_{3/2}$	(152 ±71) ms [41]	(21 ±5) ms	0.14 ±0.07	0.48
	1340 ±8	$0h_{11/2}$	(860 ±290) ms [41]	(280 ±50) ms	0.32 ±0.11	0.23
$^{167}_{77}Ir_{90}$	1086 ±6	$2s_{1/2}$	(110 ±15) ms [41]	(36 ±7) ms	0.33 ±0.08	0.51
	1261 ±7	$0h_{11/2}$	(7.5 ±1.9) s [41]	(2.0 ±0.4) ms	0.27 ±0.09	0.23
$^{171}_{79}Au_{92}$	1718 ±6	$0h_{11/2}$	(2.22 ±0.29) ms [41]	(0.35 ±0.04) ms	0.16 ±0.03	0.14
$^{185}_{83}Bi_{98}$	1611 ±9	$2s_{1/2}$ (?)	(44 ±16) μs [5]	(3.2 ±0.6) μs	0.072 ±0.03	0
	1611 ±9	$0h_{9/2}$ (?)	(44 ±16) μs [5]	(21000 ±4000) μs	470 ±190	1

For odd-odd nuclei the agreement between experiment and theory is fair. There are three clear deviations from theoretical predictions: ^{112}Cs (which is expected to be deformed), and the alleged $\pi d_{3/2}\nu f_{7/2}$ states in ^{160}Re [42] and ^{166}Ir [41]. As seen in Table IV, it is the $2s_{1/2}$ orbital, rather than the $1d_{3/2}$ orbital that has been observed in neighboring odd-even nuclei. However, as discussed in Ref. [41], the neutron-proton (np) residual interaction in the $\pi d_{3/2}\nu f_{7/2}$ configuration is strong enough to push the resulting two-quasiparticle state down in energy. As known from the heavier nuclei (see, e.g., Ref. [24]), the $2s_{1/2}$ and $1d_{3/2}$ orbitals are almost degenerate; they form a pseudo-spin $\tilde{p}_{1/2,3/2}$ doublet. However, as immediately seen in Table IV, by assuming the $2s_{1/2}$ orbital in ^{160}Re and ^{166}Ir, one obtains even shorter theoretical half-lives; the extracted experimental spectroscopic factors are smaller by an order of magnitude. Therefore, one is led to the conclusion, that the quenching seen experimentally does not have a simple single-particle origin.

Another possibility was suggested in Ref. [42]. Namely, the authors speculated that ^{160}Re is slightly deformed. In our study, the interaction between nuclear core and odd proton is described by the spherical WS model. Consequently, all higher-order couplings (e.g., between one-quasiparticle and three-quasiparticle states in odd-Z, odd-A nuclei) are effectively taken into account, *provided* that they do not break intrinsic spherical symmetry. For odd-odd nuclei, however, the residual np interaction can lead to deformed shapes already in the lowest order. For instance, in the above case of ^{160}Re and ^{166}Ir, the quadrupole component of the np interaction is expected to mix the near-lying $\pi d_{3/2}\nu f_{7/2}$ and $\pi s_{1/2}\nu f_{7/2}$ configurations, hence reduce the single-particle

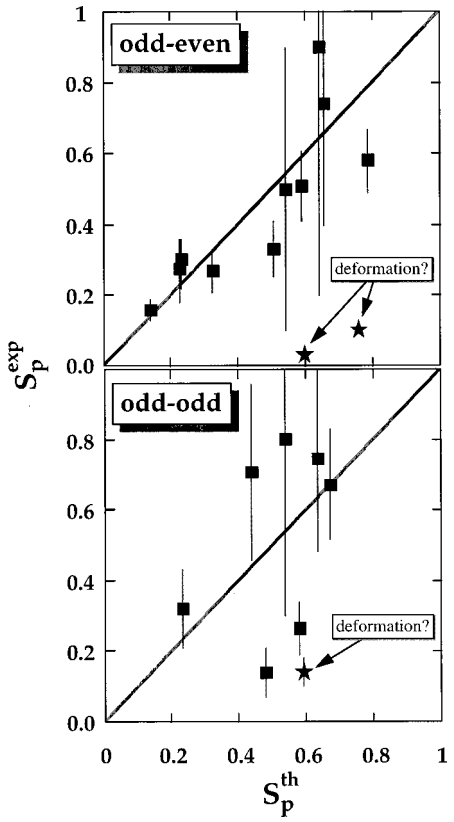

FIG. 8. Correlation between the experimental proton spectroscopic factors $S_p^{\rm exp}$ deduced from measured ground-state proton decay half-lives [Eq. (29)] and theoretical values $S_p^{\rm th}$ obtained in the BCS theory [Eq. (31)]. Top: odd-Z, even-N proton emitters; bottom odd-odd proton emitters. The nuclei expected to be deformed are indicated by stars.

strength (see Ref. [38] for the ^{109}I case).

The coupling between one-quasiparticle and three-quasiparticle states has been invoked in Ref. [5] to explain the ground-state proton decay of ^{185}Bi. Here, the two configurations of interest are (i) the spherical $0h_{9/2}$ one-quasiparticle configuration, and (ii) the *deformed* state associated with the three-quasiparticle configuration $2s_{1/2}^{-1}0h_{9/2}^{2}$. An additional complication comes from the fact that the daughter nucleus ^{184}Pb has, most likely, a low-lying deformed state that is slightly admixed to the spherical ground state. Therefore, in addition to the effects of configuration mixing of the valence proton orbital, one here also expects a strong rearrangement of the core configuration giving rise to an additional quenching of single-particle strength. Clearly, a spherical one-body approach is not very appropriate for tackling such a complex situation.

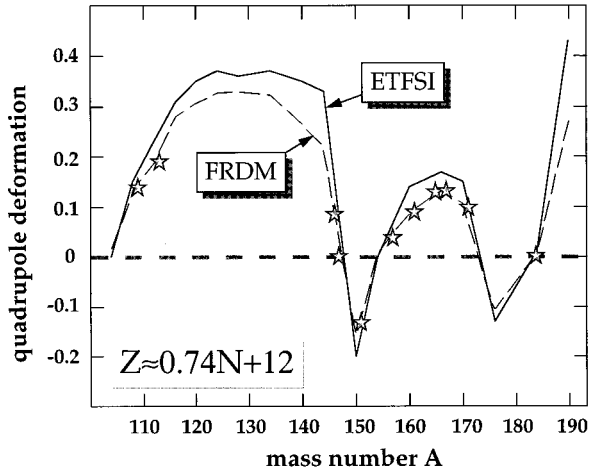

FIG. 9. Theoretical equilibrium quadrupole deformations of Refs. [36] (FRDM) and [37] (ETFSI) along the $Z\approx 0.74N+12$ line. The known proton emitters are indicated by stars.

VI. SUMMARY

Three theories for describing the ground-state proton radioactivity in spherical nuclei have been investigated: the distorted wave Born approximation, the two-potential approach, and the quasiclassical method. In spite of the different degrees of sophistication in these models, they were nonetheless found to give rather similar results.

The two-potential approximation, in the version by Gurvitz [13] gives a remarkably close agreement with the DWBA results when the (very small) energy shift is ignored. We have also checked that a simplified version of the TPA, in which one replaces in Eq. (19) the regular scattering wave $\chi_\ell(r)$ by the regular Coulomb wave function $F_\ell(r)$ (the TPA2 variant), gives results which usually do not deviate from DWBA by more than 10%. This observation may have important consequences if the two-potential method is generalized to the deformed case. The results of the semiclassical method are of the same quality as those with the TPA2. We note, however, that the proper treatment of the normalization (24) is necessary for a quantitative description of the data.

The sensitivity of the calculated half-lives on variations in model parameters has been studied. In general, proton emission half-lives depend mainly on the proton separation energy and orbital angular momentum, but rather weakly on the details of intrinsic structure of proton emitters, e.g., on the parameters of the proton potential at least at a qualitative level (factors of 2–3). However, for a detailed description of experimental data, better than just an order-of-magnitude *qualitative* estimate, the average proton potential has to be selected carefully. In this context, the Woods-Saxon potential of Becchetti and Greenlees [21] seems to be a preferred choice.

Proton radioactivity occurs in nuclei far from the beta stability valley where the detailed spectroscopic studies are difficult. Since proton emission half-lives are insensitive to nuclear structure details, studies of proton emitters provide us with invaluable and fairly precise information on shell structure of exotic nuclei where the nuclear binding ends. Our calculations demonstrate that a simple one-body approach to the tunneling problem, supplemented by a BCS treatment of correlations, gives a *quantitative* description of experimental proton half-lives (or single-particle spectroscopic factors) in most cases.

The strong dependence on the orbital angular momentum also suggests that the ℓ mixing due to residual interaction or,

e.g., induced by static deformation, might be not only observable, but also recognizable. As studies of exotic nuclei progress, it will be very important to determine the empirical ordering of different single-particle states near and beyond the drip-line, to classify excited states, and, possibly, to investigate the competition between the proton radioactivity and other decay modes (such as gamma decay). Theoretically, the extensions of the formalism to deformed systems and to vibrational nuclei are the necessary next steps. One interesting possibility is the strong coupling scheme based on the coupled-channel formalism for deformed proton emitters proposed in Refs. [38–40]. However, we hope that the results of the present spherical ''test-case'' study will be useful for developing other simpler techniques. The quantitative agreement with experimental data for spherical proton emitters obtained in our study suggests that it will indeed be possible to obtain, from half-lives of deformed proton emitters, a rather clear spectroscopic information on the angular momentum decomposition of single-proton Nilsson orbitals.

ACKNOWLEDGMENTS

We thank C.R. Bingham, C.N. Davids, S. Hofmann, and P.J. Woods for comments and for providing information about experimental data prior to publication. Useful discussions with G.R. Satchler are gratefully acknowledged. We thank the Institute for Nuclear Theory at the University of Washington for its hospitality and the U.S. Department of Energy for partial support during the completion of this work. The Joint Institute for Heavy Ion Research has as member institutions the University of Tennessee, Vanderbilt University, and the Oak Ridge National Laboratory; it is supported by the members and by the U.S. Department of Energy through Contract No. DE-FG05-87ER40361 with the University of Tennessee. In addition, partial support was provided by the U.S. Department of Energy under the Grant No. DE-FG05-92ER40694 (PBS) and No. DE-FG02-96ER40963 (WN). Oak Ridge National Laboratory is managed for the U.S. Department of Energy by Lockheed Martin Energy Research Corporation under Contract No. DE-AC05-96OR22464.

[1] S. Hofmann, in *Particle Emission from Nuclei*, edited by D. N. Poenaru and M. Ivascu (CRC, Boca Raton, 1989), Vol. 2, Chap. 2.
[2] S. Hofmann, Radiochim. Acta **70/71**, 93 (1995).
[3] S. Hofmann, in *Nuclear Decay Modes*, edited by D. N. Poenaru and W. Greiner (IOP, Bristol, 1996).
[4] C. N. Davids, P. J. Woods, J. C. Batchelder, C. R. Bingham, D. J. Blumenthal, L. T. Brown, B. C. Busse, L. F. Conticchio, T. Davidson, S. J. Freeman, M. Freer, D. J. Henderson, R. J. Irvine, R. D. Page, H. T. Penttilä, A. V. Ramayya, D. Seweryniak, K. S. Toth, W. B. Walters, A. H. Wuosmaa, and B. E. Zimmerman, Proceedings of the International Conference on Exotic Nuclei and Atomic Masses, Arles, France, 1995, edited by M. de Saint Simon and O. Sorlin (Editions Frontières, Gif-sur-Yvette, 1996).
[5] C. N. Davids, P. J. Woods, H. T. Penttilä, J. C. Batchelder, C. R. Bingham, D. J. Blumenthal, L. T. Brown, B. C. Busse, L. F. Conticchio, T. Davinson, D. J. Henderson, D. Seweryniak, K. S. Toth, W. B. Walters, and B. E. Zimmerman, Phys. Rev. Lett. **76**, 592 (1996).
[6] H. Feshbach, *Theoretical Nuclear Physics: Nuclear Reactions* (Wiley, New York, 1992).
[7] G. R. Satchler, *Direct Nuclear Reactions* (Oxford University Press, New York, 1983).
[8] N. K. Glendenning, *Direct Nuclear Reactions* (Academic, New York, 1983).
[9] S. G. Kadmenskiĭ and V. E. Kalechtis, Sov. J. Nucl. Phys. **12**, 37 (1971).
[10] W. F. Feix and E. R. Hilf, Phys. Lett. **120B**, 14 (1983).
[11] Y. B. Zel'dovich, Sov. Phys. JETP **12**, 542 (1961).
[12] W. J. Romo, Nucl. Phys. **A419**, 333 (1984).
[13] S. A. Gurvitz, Phys. Rev. A **38**, 1747 (1988).
[14] A. I. Baz, Ya. B. Zel'dovich, and A. M. Perelomov, *Scattering Reactions and Decay in Nonrelativistic Quantum Mechanics* (Israel Program for Scientific Translations, Jerusalem, 1969).
[15] S. G. Kadmenskiĭ and V. G. Khlebostroev, Sov. J. Nucl. Phys. **18**, 505 (1974).
[16] R. M. de Vries, Comput. Phys. Commun. **11**, 249 (1976).
[17] S. A. Gurvitz and G. Kalbermann, Phys. Rev. Lett. **59**, 262 (1987).
[18] D. F. Jackson and M. Rhoades-Brown, Ann. Phys. (N.Y.) **105**, 151 (1977).
[19] T. Berggren and P. Olanders, Nucl. Phys. **A473**, 189 (1987).
[20] B. Buck, A. C. Merchant, and S. M. Perez, Phys. Rev. C **45**, 1688 (1992).
[21] F. D. Becchetti, Jr. and G. W. Greenlees, Phys. Rev. **182**, 1190 (1969).
[22] J. Dudek, Z. Szymański, and T. Werner, Phys. Rev. C **23**, 920 (1981).
[23] S. Ćwiok, J. Dudek, W. Nazarewicz, J. Skalski, and T. Werner, Comput. Phys. Commun. **46**, 379 (1987).
[24] W. Nazarewicz, M. A. Riley, and J. D. Garrett, Nucl. Phys. **A512**, 61 (1990).
[25] W. Nazarewicz, J. Dudek, R. Bengtsson, T. Bengtsson, and I. Ragnarsson, Nucl. Phys. **A435**, 397 (1985).
[26] W. Nazarewicz, J. Dobaczewski, T. R. Werner, J. A. Maruhn, P.-G. Reinhard, K. Rutz, C. R. Chinn, A. S. Umar, and M. R. Strayer, Phys. Rev. C **53**, 740 (1996).
[27] S. G. Nilsson and I. Ragnarsson, *Shapes and Shells in Nuclear Structure* (Cambridge University Press, Cambridge, England, 1995).
[28] D. N. Poenaru and W. Greiner, in *Handbook of Nuclear Properties*, edited by D. N. Poenaru and W. Greiner (Clarendon, Oxford, 1996), p. 131.
[29] P. J. Sellin, P. J. Woods, T. Davinson, N. J. Davis, K. Livingston, R. D. Page, A. C. Shotter, S. Hofmann, and A. N. James, Phys. Rev. C **47**, 193 (1993).
[30] V. I. Goldansky, Nucl. Phys. **19**, 482 (1960).
[31] B. A. Brown and P. G. Hansen, Phys. Lett. B **381**, 391 (1996).
[32] A. Bohr and B. R. Mottelson, Nuclear Structure (W.A. Ben-

jamin, New York, 1969), Vol. 1.
[33] K. Heyde, *The Nuclear Shell Model* (Springer Verlag, Berlin, 1990).
[34] R. A. Sorensen and E. D. Lin, Phys. Rev. C **142**, 729 (1966).
[35] J. Dudek, A. Majhofer, and J. Skalski, J. Phys. G **6**, 447 (1980).
[36] P. Möller, J. R. Nix, W. D. Myers, and W. J. Swiatecki, At. Data Nucl. Data Tables **59**, 185 (1995).
[37] Y. Aboussir, J. M. Pearson, A. K. Dutta, and F. Tondeur, At. Data Nucl. Data Tables **61**, 127 (1995).
[38] V. P. Bugrov and S. G. Kadmenskiĭ, Sov. J. Nucl. Phys. **49**, 967 (1989).
[39] D. D. Bogdanov, V. P. Bugrov, and S. G. Kadmenskiĭ, Sov. J. Nucl. Phys. **52**, 229 (1990).
[40] S. G. Kadmenskiĭ and V. P. Bugrov, Phys. At. Nucl. **59**, 399 (1996).
[41] C. N. Davids, P. J. Woods, J. C. Batchelder, C. R. Bingham, D. J. Blumenthal, L. T. Brown, B. C. Busse, L. F. Conticchio, T. Davinson, S. J. Freeman, D. J. Henderson, R. J. Irvine, R. D. Page, H. T. Penttilä, D. Seweryniak, K. S. Toth, W. B. Walters, and B. E. Zimmerman, Phys. Rev. C **55**, 2255 (1997).
[42] R. D. Page, P. J. Woods, R. A. Cunningham, T. Davinson, N. J. Davis, S. Hofmann, A. N. James, K. Livingston, P. J. Sellin, and A. C. Shotter, Phys. Rev. Lett. **68**, 1287 (1992).
[43] R. D. Page, P. J. Woods, R. A. Cunningham, T. Davinson, N. J. Davis, A. N. James, K. Livingston, P. J. Sellin, and A. C. Shotter, Phys. Rev. Lett. **72**, 1798 (1994).
[44] K. Livingston, P. J. Woods, T. Davinson, N. J. Davis, S. Hofmann, A. N. James, R. D. Page, P. J. Sellin, and A. C. Shotter, Phys. Lett. B **312**, 46 (1993).
[45] K. S. Toth, D. C. Sousa, P. A. Wilmarth, J. M. Nitschke, and K. S. Vierinen, Phys. Rev. C **47**, 1804 (1993).
[46] R. D. Page, P. J. Wood, R. A. Cunningham, T. Davinson, N. J. Davis, A. N. James, K. Livingston, P. J. Sellin, and A. C. Shotter, Phys. Rev. C **53**, 660 (1996).
[47] R. J. Irvine, C. N. Davids, P. J. Woods, D. J. Blumenthal, L. T. Brown, L. F. Conticchio, T. Davinson, D. J. Henderson, J. A. Mackenzie, H. T. Penttilä, D. Seweryniak, and W. B. Walters, Phys. Rev. C **55**, R1621 (1997).